Front. Phys. 13(4), 136702 (2018)
https://doi.org/10.1007/s11467-018-0802-2

RESEARCH ARTICLE

Polarons in alkaline-earth-like atoms with multiple background Fermi surfaces

Jin-Ge Chen[1], **Yue-Ran Shi**[1], **Xiang Zhang**[1,†], **Wei Zhang**[1,2,‡]

[1] *Department of Physics, Renmin University of China, Beijing 100872, China*
[2] *Beijing Key Laboratory of Opto-electronic Functional Materials and Micro-nano Devices, Renmin University of China, Beijing 100872, China*
Corresponding authors. E-mail: [†] *siang.zhang@ruc.edu.cn,* [‡] *wzhangl@ruc.edu.cn*
Received April 11, 2018; accepted May 14, 2018

We study the impurity problem in a Fermi gas of ^{173}Yb atoms near an orbital Feshbach resonance (OFR), where a single moving particle in the $^3P_0$ state interacts with two background Fermi seas of particles in different nuclear states of the ground $^1S_0$ manifold. By employing wave function ansatz to molecule and polaron states, we investigate various properties of the molecule, the attractive polaron, and the repulsive polaron states. In comparison to the case where only one Fermi sea is populated, we find that the presence of an additional Fermi sea acts as an energy shift between the two channels of the OFR. In addition, quantum fluctuations near the Fermi level can also induce sizable effects to various properties of the attractive and repulsive polarons.

Keywords Fermi gas, alkaline-earth atoms, orbital Feshbach resonance, polaron

PACS numbers 67.85.Lm, 03.75.Ss, 05.30.Fk

1 Introduction

Ever since the orbital Feshbach resonance (OFR) was proposed theoretically [1] and realized experimentally [2, 3] in ^{173}Yb atoms, much effort has been devoted to alkaline-earth(-like) atoms which greatly enriched the scope of quantum simulation in these systems [4–15]. Among these studies, the study of polaron and molecule states in a system of an impurity fermion immersed atop a Fermi sea consisting of particles of another species is of particular interest [13–15]. For alkali atoms near a magnetic Feshbach resonance, such an impurity problem has caught great attention in the past decade [16–27] and is considered to be closely related to itinerant ferromagnetism [28–34] in Fermi systems with large polarization. In the context of alkaline-earth(-like) atoms near an OFR, recent studies considered the configuration of a single impurity in the excited orbital state interacting with a majority Fermi sea in one of the ground orbital states and discussed various properties of the polaron and molecule states [13–15]. From these studies, it is understood that the polaron and molecule states in such a system are drastically different from those in alkali atoms because the OFR in this case is a narrow resonance with two-channel nature and a spin-exchange interaction.

In this manuscript, we fully employ the multichannel nature of an OFR and consider a generalized impurity problem, where a single atom in the excited orbital state interacts with two background Fermi seas in the ground orbital states with different spin indices. Taking the atoms of ^{173}Yb as a concrete example, the ground (denoted as $|g\rangle$) and excited ($|e\rangle$) orbital states correspond to the two clock-state manifolds $^1S_0$ and $^3P_0$, respectively. As the total electronic angular momentum is zero ($J = 0$), the nuclear and the electronic spin degrees of freedom are decoupled such that the states with different nuclear magnetic numbers m_I can be labeled as pseudospins $|\uparrow\rangle$ and $|\downarrow\rangle$, which are Zeeman shifted in the presence of an external magnetic field. Without loss of generality, we may refer to the scattering channel consisting of $|g\downarrow\rangle$ and $|e\uparrow\rangle$ states as the open channel, and the one consisting of $|g\uparrow\rangle$ and $|e\downarrow\rangle$ as the closed channel. Due to the differential Zeeman shift between the two channels, an OFR occurs when a two-body bound state within one channel becomes degenerate with the threshold of the other, leading to a crossover from the Bardeen-Cooper-Schrieffer (BCS) regime to the Bose-Einstein condensate

*arXiv: 1801.09375.

(BEC) regime.

The system discussed in this manuscript is illustrated in Fig. 1, where a mobile atom in the $|e\uparrow\rangle$ state is interacting with the two ground state Fermi seas of $|g\uparrow\rangle$ and $|g\downarrow\rangle$ atoms. Next, employing the Chevy-like ansatz for the polaron state with one particle-hole fluctuation and for the bare molecule state without particle-hole fluctuations [16, 17], we characterize various properties of the attractive polaron and the molecule states including the eigen energy, the wave function, and the effective mass. We specifically demonstrate that there exists a molecule-attractive polaron transition across the OFR, with the transition point varying with the Fermi levels. We further focus on the quasiparticle excitation called the repulsive polaron and investigate the corresponding spectral function, eigen energy, wave function, quasiparticle residue, effective mass, and decay rate. From these results, we conclude that the presence of an extra Fermi sea acts mainly as an energy offset of atomic states, which can be understood as an effective shift of the inter-channel detuning. Meanwhile, the fluctuation around the Fermi level induced by interaction can also blur the resonant-scattering processes and smoothen the kink structure in various quantities of the repulsive polaron.

The remainder of this paper is organized as follows. In Section 2, we present the Hamiltonian of the system under consideration and introduce the formalism of the wave function ansatz. The properties of the molecule and attractive polaron states throughout the resonance region are discussed in Section 3. Then we focus on the repulsive polaron state and discuss its properties in Section 4. In Section 5, we summarize our study.

2 Formalism

We consider the problem of a single impurity immersed in a two-component Fermi gas of alkaline-earth-like atoms across an OFR. The system is composed of atoms in two electronic orbital states labeled by $(g,\ e)$ and two nuclear spin states by $(\uparrow,\ \downarrow)$, where the open and the closed channels are formed by the combinations $|o\rangle = \frac{1}{\sqrt{2}}(|g\downarrow;e\uparrow\rangle - |e\uparrow;g\downarrow\rangle)$ and $|c\rangle = \frac{1}{\sqrt{2}}(|g\uparrow;e\downarrow\rangle - |e\downarrow;g\uparrow\rangle)$, respectively. The Hamiltonian of the system can be written as

$$\begin{aligned}\hat{H} = &\sum_{\boldsymbol{k}} \epsilon_{\boldsymbol{k}} (a^{\dagger}_{\boldsymbol{k}g\downarrow} a_{\boldsymbol{k}g\downarrow} + a^{\dagger}_{\boldsymbol{k}e\downarrow} a_{\boldsymbol{k}e\downarrow}) \\ &+ \sum_{\boldsymbol{k}} (\epsilon_{\boldsymbol{k}} + \delta_g)(a^{\dagger}_{\boldsymbol{k}g\uparrow} a_{\boldsymbol{k}g\uparrow}) \\ &+ \sum_{\boldsymbol{k}} (\epsilon_{\boldsymbol{k}} + \delta_e)(a^{\dagger}_{\boldsymbol{k}e\uparrow} a_{\boldsymbol{k}e\uparrow}) + \hat{H}_{\rm int}. \end{aligned} \tag{1}$$

Here $a^{\dagger}_{\boldsymbol{k}p\sigma}$ and $a_{\boldsymbol{k}p\sigma}$ are creation and annihilation operators associated with fermions with three-dimensional linear momentum $\boldsymbol{k}$, electronic orbital state $p = (e, g)$, and nuclear spin (pseudo-spin) state $\sigma = (\uparrow, \downarrow)$. Due to the differential Zeeman shift, the single-particle dispersions $\epsilon_{\boldsymbol{k}}$ in the open and closed channels are shifted by detunings δ_e and δ_g respectively, as illustrated in Fig. 1. An OFR occurs as the bound state energy within the closed channel becomes degenerate with the scattering threshold of the open channel, or vice versa, by tuning $\delta_e - \delta_g$.

The interaction Hamiltonian can be expressed in the basis of the orbital symmetric state $|+\rangle = \frac{1}{2}(|ge\rangle + |eg\rangle) \otimes (|\downarrow\uparrow\rangle - |\uparrow\downarrow\rangle) = \frac{1}{\sqrt{2}}(|o\rangle - |c\rangle)$ and the orbital antisymmetric state $|-\rangle = \frac{1}{2}(|ge\rangle - |eg\rangle) \otimes (|\downarrow\uparrow\rangle + |\uparrow\downarrow\rangle) = \frac{1}{\sqrt{2}}(|o\rangle + |c\rangle)$, and takes the following form [13]

$$\begin{aligned}\hat{H}_{\rm int} = \sum_{\boldsymbol{q}} \Big[&\frac{g_+}{2} \hat{A}^{\dagger}_{\boldsymbol{q},+} \hat{A}_{\boldsymbol{q},+} + \frac{g_-}{2} \Big(\hat{A}^{\dagger}_{\boldsymbol{q},-} \hat{A}_{\boldsymbol{q},-} \\ &+ \hat{A}^{\dagger}_{\boldsymbol{q},\downarrow} \hat{A}_{\boldsymbol{q},\downarrow} + \hat{A}^{\dagger}_{\boldsymbol{q},\uparrow} \hat{A}_{\boldsymbol{q},\uparrow} \Big) \Big] \end{aligned} \tag{2}$$

with the operators defined as

$$\begin{aligned}\hat{A}_{\boldsymbol{q},+} &= \sum_{\boldsymbol{k}} (a_{-\boldsymbol{k}+\boldsymbol{q},g\downarrow} a_{\boldsymbol{k}+\boldsymbol{q},e\uparrow} - a_{-\boldsymbol{k}+\boldsymbol{q},g\uparrow} a_{\boldsymbol{k}+\boldsymbol{q},e\downarrow}), \\ \hat{A}_{\boldsymbol{q},-} &= \sum_{\boldsymbol{k}} (a_{-\boldsymbol{k}+\boldsymbol{q},g\downarrow} a_{\boldsymbol{k}+\boldsymbol{q},e\uparrow} + a_{-\boldsymbol{k}+\boldsymbol{q},g\uparrow} a_{\boldsymbol{k}+\boldsymbol{q},e\downarrow}), \\ \hat{A}_{\boldsymbol{q},\downarrow} &= \sum_{\boldsymbol{k}} (a_{-\boldsymbol{k}+\boldsymbol{q},g\downarrow} a_{\boldsymbol{k}+\boldsymbol{q},e\downarrow} + a_{-\boldsymbol{k}+\boldsymbol{q},g\downarrow} a_{\boldsymbol{k}+\boldsymbol{q},e\downarrow}), \\ \hat{A}_{\boldsymbol{q},\uparrow} &= \sum_{\boldsymbol{k}} (a_{-\boldsymbol{k}+\boldsymbol{q},g\uparrow} a_{\boldsymbol{k}+\boldsymbol{q},e\uparrow} + a_{-\boldsymbol{k}+\boldsymbol{q},g\uparrow} a_{\boldsymbol{k}+\boldsymbol{q},e\uparrow}). \end{aligned} \tag{3}$$

The interaction strengths $g_{\pm}$ are related to the corresponding s-wave scattering lengths $a_{\pm}$ via the standard renormalization relation $1/g_{\pm} = 1/g^p_{\pm} - \sum_{\boldsymbol{k}} 1/(2\epsilon_{\boldsymbol{k}})$, where $g^p_{\pm} = 4\pi\hbar^2 a_{\pm}/m$ are physical interaction parameters with m as the atomic mass. Throughout the paper, we consider the atom of ^{173}Yb as a particular example, where the scattering lengths $a_+ = 1900a_0$ and $a_- = 200a_0$ with a_0 as the Bohr radius [3, 8].

The fermion impurity problem, by definition, is to impose the minority impurity atoms against a majority Fermi sea formed by fermions of another type. In this study, we take advantage of the multistate nature of

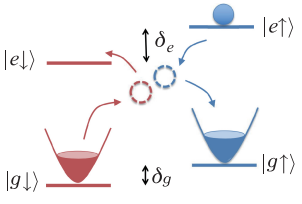

Fig. 1 Level diagram of an orbital Feshbach resonance. An impurity $|e\uparrow\rangle$ is immersed in a two-component ($|g\downarrow\rangle$ and $|g\uparrow\rangle$) Fermi gas of alkaline-earth(-like) atoms. The impurity can interact with one atom in the $|g\downarrow\rangle$ state and the two particles in the open-channel can be scattered into the closed channel ($|g\uparrow\rangle$ and $|e\downarrow\rangle$ states) through a spin-exchange interaction.

OFR and consider a generalized configuration of a single impurity in the $|e\uparrow\rangle$ state immersed in two Fermi seas of $N_\downarrow$ atoms in the $|g\downarrow\rangle$ state (open channel) and $N_\uparrow$ atoms in the $|g\uparrow\rangle$ state (closed channel), as illustrated in Fig. 1. We study the molecule and polaron states within such a system using the Chevy-like ansatz [16, 17], which is equivalent with the summation of particle-particle ladder diagrams for the vertex in a nonself-consistent T-matrix approach [17].

In a molecule state, the $|e\uparrow\rangle$ impurity scatters one atom out of the $|g\downarrow\rangle_{N\downarrow}$ Fermi sea and the two atoms form a bound state; or they can be scattered into the closed channel through the spin-flipping processes of the interaction. We then assume a trial wave function as

$$|M\rangle_{\boldsymbol{Q}} = \sum_{|\boldsymbol{k}|>k_{\downarrow F}} \alpha_{\boldsymbol{k}} a^\dagger_{\boldsymbol{Q}-\boldsymbol{k},e\uparrow} a^\dagger_{\boldsymbol{k},g\downarrow} |g\downarrow\rangle_{N\downarrow-1}|g\uparrow\rangle_{N\uparrow} + \sum_{|\boldsymbol{k}|>k_{\uparrow F}} \beta_{\boldsymbol{k}} a^\dagger_{\boldsymbol{Q}-\boldsymbol{k},e\downarrow} a^\dagger_{\boldsymbol{k},g\uparrow} |g\downarrow\rangle_{N\downarrow-1}|g\uparrow\rangle_{N\uparrow}, \quad (4)$$

where $\mathbf{Q}$ denotes the center-of-mass momentum, and $\alpha_{\boldsymbol{k}}$ and $\beta_{\boldsymbol{k}}$ are the coefficients of the open and closed channels, respectively. Notice that the summations over linear momentum $\boldsymbol{k}$ run over states above the corresponding Fermi seas with Fermi momenta $k_{\downarrow F}$ and $k_{\uparrow F}$.

By evaluating the energy expectation $\tilde{E}_M(\boldsymbol{Q}) = {}_{\boldsymbol{Q}}\langle M|\hat{H}|M\rangle_{\boldsymbol{Q}}$ and taking the variations of $\alpha_{\boldsymbol{k}}$ and $\beta_{\boldsymbol{k}}$, we can derive the equation for the energy of the molecule state [13]

$$\frac{1}{g^p_- g^p_+} + \frac{1}{2}\left(\frac{1}{g^p_-} + \frac{1}{g^p_+}\right)\left(\Theta_{\boldsymbol{Q}} + \Theta'_{\boldsymbol{Q}} - 2\Lambda_c\right) + (\Theta_{\boldsymbol{Q}} - \Lambda_c)(\Theta'_{\boldsymbol{Q}} - \Lambda_c) = 0, \quad (5)$$

where

$$\Theta'_{\boldsymbol{Q}} = \sum_{|\boldsymbol{k}|>k_{\downarrow F}} \frac{1}{\epsilon_{\boldsymbol{k}} + \epsilon_{\boldsymbol{Q}-\boldsymbol{k}} + \delta_e - E_M},$$
$$\Theta_{\boldsymbol{Q}} = \sum_{|\boldsymbol{k}|>k_{\uparrow F}} \frac{1}{\epsilon_{\boldsymbol{k}} + \epsilon_{\boldsymbol{Q}-\boldsymbol{k}} + \delta_g - E_M}, \quad (6)$$

and $\Lambda_c = \sum_{\boldsymbol{k}} 1/(2\epsilon_{\boldsymbol{k}})$. Notice that in the expressions above, we shift the energy reference to $E_M = \tilde{E}_M - \sum_{|\boldsymbol{k}|<k_{\downarrow F}} \epsilon_{\boldsymbol{k}} - \sum_{|\boldsymbol{k}|<k_{\uparrow F}} (\epsilon_{\boldsymbol{k}} + \delta_g)$. With such a reference, the threshold energy $E_{\rm th}$ equals δ_e for a noninteracting zero-momentum impurity $|e\uparrow\rangle$ on the two Fermi surfaces of $|g\downarrow\rangle_{N\downarrow}$ and $|g\uparrow\rangle_{N\uparrow}$.

For the polaron state, we consider the following ansatz wave function

$$|P\rangle_{\boldsymbol{Q}} = \left(\gamma a^\dagger_{\boldsymbol{Q}e\uparrow} + \sum_{\substack{|\boldsymbol{k}|>k_{\downarrow F}\\ |\boldsymbol{q}|<k_{\downarrow F}}} \alpha_{\boldsymbol{k}\boldsymbol{q}} a^\dagger_{\boldsymbol{Q}+\boldsymbol{q}-\boldsymbol{k},e\uparrow} a^\dagger_{\boldsymbol{k},g\downarrow} a_{\boldsymbol{q},g\downarrow} + \sum_{\substack{|\boldsymbol{k}|>k_{\uparrow F}\\ |\boldsymbol{q}|<k_{\downarrow F}}} \beta_{\boldsymbol{k}\boldsymbol{q}} a^\dagger_{\boldsymbol{Q}+\boldsymbol{q}-\boldsymbol{k},e\downarrow} a^\dagger_{\boldsymbol{k},g\uparrow} a_{\boldsymbol{q},g\downarrow}\right)|g\downarrow\rangle_{N\downarrow}|g\uparrow\rangle_{N\uparrow}. \quad (7)$$

In this expression, the first term corresponds to a bare impurity in the $|e\uparrow\rangle$ state and two unperturbed Fermi seas, the second term represents a state with one pair of particle-hole excitation atop the $|g\downarrow\rangle_{N\downarrow}$ Fermi sea, and the third term corresponds to a state where the fermion created above $|g\downarrow\rangle_{N\downarrow}$ Fermi sea interacts with the $|e\uparrow\rangle$ impurity and both are scattered into the closed channel.

We can derive the energy equation for the polaron state following the same method as that for the molecule state, which leads to

$$E_P - \epsilon_{\boldsymbol{Q}} - \delta_e = \sum_{|\boldsymbol{q}|<k_{\downarrow F}} \left\{\frac{1}{2}\left(\frac{1}{g^p_+} + \frac{1}{g^p_-}\right) + \Gamma'_{\boldsymbol{Q}\boldsymbol{q}} - \Lambda_c - \frac{1}{4}\left(\frac{1}{g^p_+} - \frac{1}{g^p_-}\right)^2 \left[\frac{1}{2}\left(\frac{1}{g^p_+} + \frac{1}{g^p_-}\right) + \Gamma_{\boldsymbol{Q}\boldsymbol{q}} - \Lambda_c\right]^{-1}\right\}^{-1}, \quad (8)$$

where

$$\Gamma'_{\boldsymbol{Q}\boldsymbol{q}} = \sum_{|\boldsymbol{k}|>k_{\downarrow F}} \frac{1}{\epsilon_{\boldsymbol{k}} - \epsilon_{\boldsymbol{q}} + \epsilon_{\boldsymbol{Q}+\boldsymbol{q}-\boldsymbol{k}} + \delta_e - E_P},$$
$$\Gamma_{\boldsymbol{Q}\boldsymbol{q}} = \sum_{|\boldsymbol{k}|>k_{\uparrow F}} \frac{1}{\epsilon_{\boldsymbol{k}} - \epsilon_{\boldsymbol{q}} + \epsilon_{\boldsymbol{Q}+\boldsymbol{q}-\boldsymbol{k}} + \delta_g - E_P}. \quad (9)$$

Notice that one could write down another polaron state wave function ansatz $|P'\rangle_{\boldsymbol{Q}}$ from Eq. (7) by interchanging the spin indices $\uparrow\leftrightarrow\downarrow$. Since the spin-exchange interaction $\hat{H}_{\rm int}$ conserves the number of particles in each spin state, the two polaron states $|P\rangle$ and $|P'\rangle$ belong to different Hilbert spaces. As a result, the equation for the eigen energy $E_{P'}$ is completely separated from Eq. (8) and takes the same form by interchanging $\delta_e \leftrightarrow \delta_g$. In the following discussion, we focus on the $|P\rangle$ state without loss of generality. We further assume $\delta_g = 0$ as a trivial shift of energy reference, and use the units of $k_{\downarrow F} = \hbar = 1$ and $m = 1/2$ for a gas of ^{173}Yb atoms with a number density $n_\downarrow = 2\times10^{13}$ cm^{-3} for the $|g\downarrow\rangle$ state.

3 Molecule and attractive polaron states

We first study the case of zero center-of-mass momentum $\boldsymbol{Q} = 0$, and solve Eq. (5) and (8) to obtain the energies of the molecule and polaron states. Notice that for polarons, there could exist two branches of solutions

with energies below and above the threshold energy $E_{\rm th}$, which correspond to the attractive and repulsive polaron states, respectively. In this section, we focus on the attractive polaron branch, discuss its transition to the molecule state, and leave the study of repulsive polaron to Section 4.

In Fig. 2, we show the energies of the molecule and attractive polaron states with $\boldsymbol{Q}=0$ by varying the Fermi level of $k_{\uparrow F}$. Figures 2(a)–(c) confirm that for all values of $k_{\uparrow F}$, the ground state is always the attractive polaron state when δ_e is far negative, and turns into the molecule state as δ_e increases beyond a transition point δ_e^c. The transition points for the three cases illustrated in Fig. 2 are all within the BEC side of the OFR, with (a) $\delta_e^c/E_{\downarrow F}=-2.28$, $1/(k_{\downarrow F}a_c)\approx 0.81$ for $k_{\uparrow F}/k_{\downarrow F}=0$; (b) $\delta_e^c/E_{\downarrow F}=-1.50$, $1/(k_{\downarrow F}a_c)\approx 1.01$ for $k_{\uparrow F}/k_{\downarrow F}=1$; (c) $\delta_e^c/E_{\downarrow F}=2.02$, $1/(k_{\downarrow F}a_c)\approx 0.87$ for $k_{\uparrow F}/k_{\downarrow F}=2$. Here, the critical scattering length, a_c, is obtained from the relation [8]

$$a_c=\frac{-a_{s0}+\sqrt{m|\delta_e^c|/\hbar^2}(a_{s0}^2-a_{s1}^2)}{a_{s0}\sqrt{m|\delta_e^c|/\hbar^2}-1}, \tag{10}$$

where $a_{s0}=(a_-+a_+)/2$ and $a_{s1}=(a_--a_+)/2$.

To further illustrate the effect induced by the additional Fermi surface in the closed channel, we plot the transition point δ_e^c as a function of Fermi momentum $k_{\uparrow F}$ as shown in Fig. 2(d). Notice that the transition point increases monotonically with the Fermi level, reflecting the fact that the presence of the $|g\uparrow\rangle$ Fermi sea blocks the states below the Fermi energy, hence providing an effective offset of the closed channel energy δ_g. As a consequence, the open channel energy δ_e also needs to elevate by the same amount to compensate such a shift. In fact, the transition point can be well approximated by the Fermi energy $E_{\uparrow F}$ for a $k_{\uparrow F}$ not too large, as depicted in Fig. 2(d). The deviation is expected to be caused by the interaction-induced fluctuation around the Fermi level.

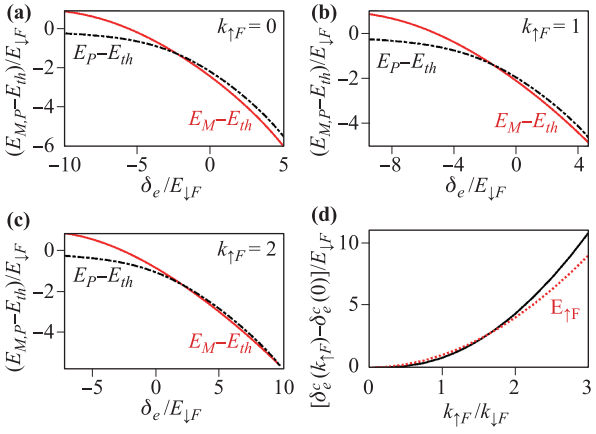

Fig. 2 **(a–c)** The eigen energies of the molecule and attractive polaron, shifted by the threshold energy $E_{\rm th}$, with zero center-of-mass momentum and (a) $k_{\uparrow F}=0$, (b) $k_{\uparrow F}=1$, (c) $k_{\uparrow F}=2$. The transition points move toward large positive δ_e with increasing $k_{\uparrow F}$. **(d)** The transition point δ_e^c varying with $k_{\uparrow F}$. The black line is the calculated result and the red dotted line is the Fermi level $E_{\uparrow F}=k_{\uparrow F}^2$. When $k_{\uparrow F}\lesssim 2$, the increase of δ_e^c almost coincides with $E_{\uparrow F}$, indicating that the Fermi level mainly acts as an energy shift. When $k_{\uparrow F}\gtrsim 2$, the deviation gradually becomes significant, due to the fluctuation effect atop the Fermi level in the closed channel.

We also calculated the fractions of wave functions in the open and closed channels for the molecule and attractive polaron states, as illustrated in Fig. 3. By comparing with results of $k_{\uparrow F}=1$ and $k_{\uparrow F}=2$, we find that the overall structures of the wave functions are very similar, except for an energy offset-shift. In particular, for both the molecule and the attractive polaron states, the wave functions are dominated by the open channel fraction in the negative δ_e region, while in the positive δ_e region the closed channel fraction becomes significantly populated. Besides, we also notice that for the attractive polaron state, the bare polaron population $|\gamma|^2$ is dominant in the BCS limit of the OFR with a large negative δ_e. When tuning towards the resonance, the fractions with particle-hole fluctuations in both the open and closed channels are enlarged due to enhanced effective interaction. When δ_e gradually increases, the wave function is dominated by the part in the closed channel $\sum|\beta|^2$ as

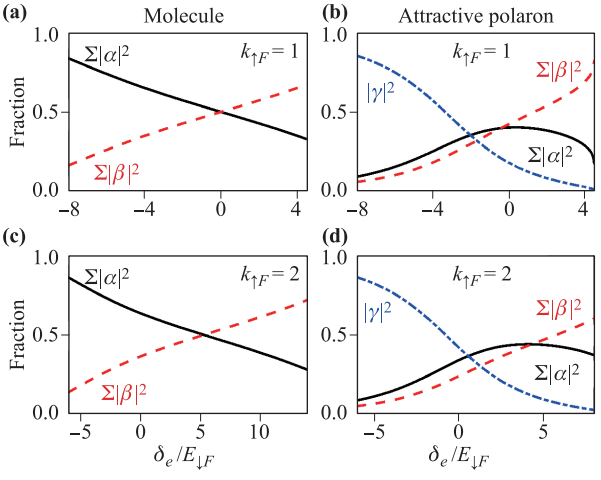

Fig. 3 The fractions of wave functions in different channels for molecule (a), (c) and attractive polaron states (b), (d) with zero center-of-mass momentum. Panels **(a)** and **(b)** are both for $k_{\uparrow F}=1$, and **(c)** and **(d)** for $k_{\uparrow F}=2$. For both the molecule and attractive polaron states, note that when δ_e is large negative (positive), the open channel contribution $\sum|\alpha|^2$ is bigger (smaller) than that of the closed channel $\sum|\beta|^2$, because the open channel is energetically favored (unfavored). For the polaron state, the bare-impurity channel $|\gamma|^2$ rapidly decreases with δ_e and approaches zero with large positive δ_e, where the particle-hole fluctuation becomes dominated as a result of strong interaction.

the open channel is largely detuned and becomes energetically unfavorable with large positive δ_e. These observations are qualitatively consistent with the results for the impurity problem with only one Fermi surface [13].

Next, we discuss the general situation of $\boldsymbol{Q} \neq 0$. For momentum not very far from $Q = 0$, we can perform a series expansion of Q in Eqs. (5) and (8) to calculate the effective masses of molecules and attractive polarons. In the region of large negative δ_e, where the attractive polaron is the ground state, the effective mass for the polaron state is positive and tends to the limiting value of $m_P^*/m \to 1$ in the BCS limit of $\delta_e \to -\infty$ as illustrated in Figs. 4(b) and (d), where the system reduces to a noninteracting impurity atom atop the two unperturbed Fermi seas. When δ_e goes beyond the transition point δ_e^c, the molecule becomes the ground state with positive effective mass. Note that as the OFR cannot be tuned into the BEC limit with $a_s \to 0^+$, the molecule state effective mass remains $m_M^*/m > 2$ in this region of δ_e, as displayed in Figs. 4(a) and (c). By further increasing δ_e to large positive values, the effective masses of both the molecule and attractive polaron states present a diverging behavior and become negative, indicating that the ground state of the system would acquire a finite center-of-mass momentum [13]. In fact, as the open channel is largely detuned above the closed channel with large positive δ_e, the impurity tends to stay in the closed channel such that the wave functions ansatz in Eqs. (4) and (7) become energetically unfavorable compared to their inter-channel counterparts with interchanging $\uparrow \leftrightarrow \downarrow$.

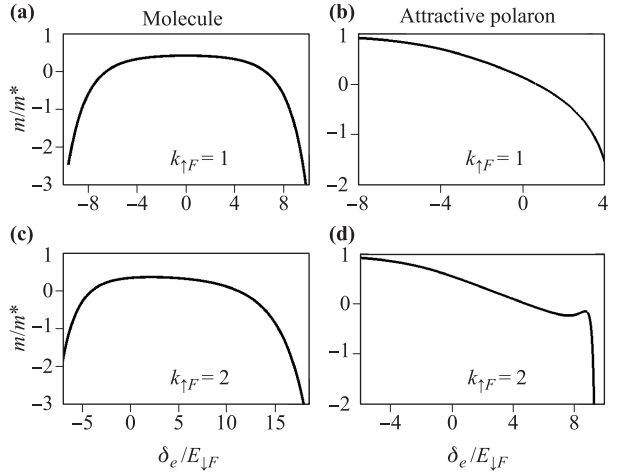

Fig. 4 **(a, c)** The inverse effective mass of molecule state with zero center-of-mass momentum for (a) $k_{\uparrow F} = 1$ and (c) $k_{\uparrow F} = 2$. In (a) the molecule effective mass diverges at $\delta_e/E_{\downarrow F} \approx -6.36$ and 6.36, both corresponding to $1/(k_{\downarrow F}a_s) \approx -0.90$, on the BCS side of the resonance. In (c) the diverging points are $\delta_e \approx -3.89$, $1/(k_{\downarrow F}a_s) \approx 0.43$ and $\delta_e \approx 11.00$, $1/(k_{\downarrow F}a_s) \approx -1.23$, respectively on the BEC side and BCS side. **(b, d)** The inverse effective mass of attractive polaron state with zero center-of-mass momentum for (b) $k_{\uparrow F} = 1$ and (d) $k_{\uparrow F} = 2$. For $k_{\uparrow F} = 1$, m_P^* diverges at $\delta_e \approx 0.62$, corresponds to the BEC side with $1/(k_{\downarrow F}a_s) \approx 1.29$. For $k_{\uparrow F} = 2$, the diverging point is $\delta_e \approx 4.80$, which is on the BEC sides with $1/(k_{\downarrow F}a_s) \approx 0.22$.

4 Repulsive polaron

In this section, we investigate the properties of the repulsive polaron branch with energy E_P above the noninteracting threshold $E_{\rm th}$. For this purpose, we write down the self-energy of a polaron with energy E_P and momentum $\boldsymbol{Q}$ as [22, 28]

$$\Sigma(\boldsymbol{Q}, E_P) = \sum_{|\boldsymbol{q}|<k_{\downarrow F}} \left[\frac{1}{2}\left(\frac{1}{g_-^p} + \frac{1}{g_+^p}\right) + \Gamma'_{\boldsymbol{Qq}} - \Lambda - \frac{1}{4}\left(\frac{1}{g_-^p} - \frac{1}{g_+^p}\right)^2 \frac{1}{\frac{1}{2}\left(\frac{1}{g_-^p} + \frac{1}{g_+^p}\right) + \Gamma_{\boldsymbol{Qq}} - \Lambda_c} \right]^{-1}, \tag{11}$$

where the functions $\Gamma'_{\boldsymbol{Qq}}$ and $\Gamma_{\boldsymbol{Qq}}$ are defined in Eq. (9). The spectral function thus takes the following form.

$$A(\boldsymbol{Q}, E_P) = -2\mathrm{Im}\frac{1}{E_P + \mathrm{i}0^+ - (\epsilon_{\boldsymbol{Q}} + \delta_e) - \Sigma(\boldsymbol{Q}, E_P)}, \tag{12}$$

where $\epsilon_{\boldsymbol{Q}} + \delta_e$ is the energy of a bare impurity with momentum $\mathbf{Q}$.

In Fig. 5, we plot the spectral function as a function of δ_e and energy E for $\boldsymbol{Q} = 0$ and $k_{\uparrow F} = 1$. There exist two branches where the spectral function is strongly peaked. The lower branch at energy $E_{P-} - E_{\rm th} < 0$ corresponds to the attractive polaron discussed in the previous section. When $\delta_e/k_{\downarrow F} \lesssim -1.5$, the attractive polaron is a stable ground state. As $\delta_e/k_{\downarrow F}$ goes beyond -1.5, the attractive branch becomes unstable towards decay into a molecule and a hole, or a molecule, two holes, and a fermion, or a molecule and other higher particle-hole excitations, which is referred as the molecule-hole continuum which is illustrated by the light-yellow area above the attractive polaron branch in the figure. The upper branch at $E_{P+} - E_{\rm th} > 0$ corresponds to the repulsive polaron. For $\delta_e/k_{\downarrow F} \lesssim -4.0$, the repulsive polaron branch merges into the molecule-hole continuum. For $-4.0 \lesssim \delta_e/k_{\downarrow F} \lesssim 0$, the repulsive polaron is a well-defined quasiparticle with strongly peaked spectral function. As $\delta_e/k_{\downarrow F} \gtrsim 0$, the repulsive polaron peak is also blurred owing to the coupling between the repulsive polaron and the closed-channel scattering states [15]. These two branches of polaron state can also be obtained from the relation

$$E_P - \delta_e = \mathrm{Re}[\Sigma(\boldsymbol{Q} = 0, E_P)]. \tag{13}$$

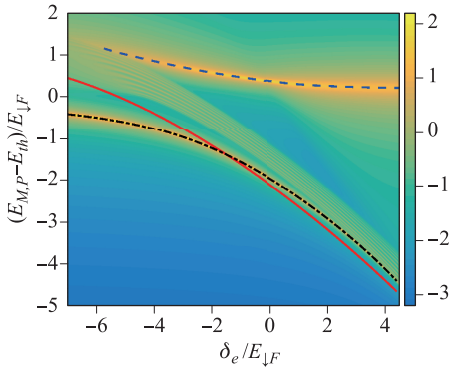

Fig. 5 False color plot of the spectral function $A(\boldsymbol{Q} = 0, E_P)$ of the polaron state as a function of detuning δ_e and energy in $\log_{10}$ scale for the case of $k_{\uparrow F} = 1$. The red solid line is the molecule energy given by Eq. (5) and the black dashed-dotted line is the attractive polaron energy given by Eq. (8), crossing at $\delta_e^c/k_{\downarrow F} \approx -1.50$. The blue dashed line denotes the repulsive polaron energy given by Eq. (13). At large negative δ_e, the repulsive polaron merges into the molecule-hole continuum which is denoted by the broad light yellow area. For positive δ_e, the repulsive polaron branch is also blurred as a result of coupling to the closed channel scattering continuum.

In fact, the solutions of the equation above are consistent with the peaks of the spectral function, as depicted in Fig. 5.

We now characterize the repulsive polaron state by calculating its populations of wave function in different channels, the quasiparticle residue, and the effective mass. The residue of a polaron state is defined as [37]

$$Z_\pm = \left\{1 - \mathrm{Re}\left[\frac{\partial\Sigma(\boldsymbol{Q}=0,E_P)}{\partial E_P}\right]_{E_{P\pm}}\right\}^{-1}, \tag{14}$$

and the effective mass as [37]

$$m^*_{P\pm} = \frac{m}{Z_\pm}\left\{1 + \mathrm{Re}\left[\frac{\partial\Sigma(\boldsymbol{Q},E_P)}{\partial \boldsymbol{Q}^2}\right]_{\substack{\boldsymbol{Q}=0,\\ E_P=E_{P\pm}}}\right\}^{-1}. \tag{15}$$

From Figs. 6(a) and (b), we find that the repulsive polaron is mainly composed by a bare impurity for δ_e not so negative, where the wave function acquires a dominating term of $|\gamma|^2$. This is consistent with the behaviors of quasiparticle residue [Fig. 6(c)] and effective mass [Fig. 6(d)], both of which indicate that the repulsive polaron tends to reduce to a bare impurity with residue $Z_+ \to 1$ and bare atomic mass $m^*_{P+} \to m = 1/2$, which is weakly interacting with the majority background Fermi seas in the limit of large positive δ_e [28].

In addition, we note that the kink structure present in the case of a single Fermi surface with $k_{\uparrow F} = 0$ is blurred and eventually smoothened by imposing an additional Fermi sea. The occurrence of these kinks is rooted from a resonance-like behavior, where the atoms in one

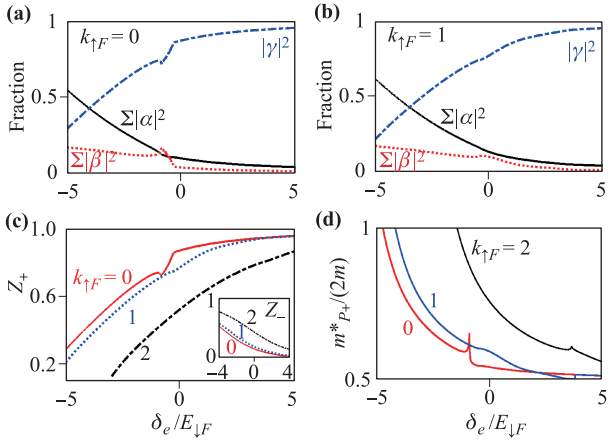

Fig. 6 **(a, b)** The populations of repulsive polaron wave function in different channels for (a) $k_{\uparrow F} = 0$ and (b) $k_{\uparrow F} = 1$ with zero center-of-mass momentum. Note that the bare impurity channel $|\gamma|^2$ becomes dominating with increasing δ_e, indicating that the interaction effect between the bare impurity and the background Fermi seas is small, as can also be implied from **(c)** the quasiparticle residue Z_+ and **(d)** the effective mass m^*_{P+}. The wave function, residue, and effective mass all have an obvious kink structure near $\delta_e/k_{\downarrow F} = -0.87$ for $k_{\uparrow F} = 0$, as a result of resonant-like scattering between the two channels [15]. In the presence of the second Fermi sea, the kinks are shifted to large δ_e to accommodate the energy offset induced by the Fermi level $E_{\uparrow F}$, and are smoothened due to the fluctuations around the Fermi sea induced by interaction. (c) Inset: Residues for attractive polarons.

channel can be resonantly scattered to the other channel when the detuning satisfies the energy-momentum conservation relations [15]. Such resonance effect is most prominent when the closed channel is empty so that the states therein are strictly forbidden if the conservation laws are unsatisfied. In the case where a Fermi sea is filled in the closed channel, the kinks are shifted due to the energy offset of the Fermi level $E_{\uparrow F}$, and also blurred because the states below the Fermi levels are no longer strictly forbidden in the presence of interaction.

As an excited quasiparticle, the repulsive polaron has a finite width in the spectral function and can decay into low-lying states. For alkali atoms, it has been shown experimentally that the dominating decay channel is the coupling to the bare impurity state in the attractive-polaron branch as the interaction is not in the deep-BEC regime [37]. For the present case of OFR, it is natural to assume that the scenario is similar in consideration of the fact that the repulsive polaron wave function mainly consists of the bare impurity, as shown in Figs. 6(a) and (b). Such a decay rate can be calculated as [15, 22, 28, 37]

$$\Gamma_{PF} = -2Z_+\mathrm{Im}[\tilde{\Sigma}(\boldsymbol{0}, E_{P+})], \tag{16}$$

where Z_+ is the residue for the repulsive polaron, and

$$\tilde{\Sigma}(\boldsymbol{Q}, E_{P+}) = \sum_{|\boldsymbol{q}|<k_{\downarrow F}} \left[\frac{1}{2}\left(\frac{1}{g_-^p} + \frac{1}{g_+^p}\right) + (1-Z_+)(\Gamma'_{\boldsymbol{Qq}} - \Lambda) - \frac{1}{4}\left(\frac{1}{g_-^p} - \frac{1}{g_+^p}\right)^2 \cdot \frac{1}{\frac{1}{2}\left(\frac{1}{g_-^p} + \frac{1}{g_+^p}\right) + \Gamma_{\boldsymbol{Qq}} - \Lambda} \right]^{-1}. \quad (17)$$

Note that in the expression for $\tilde{\Sigma}$, we have replaced the free-fermion propagator $(\Gamma'_{\boldsymbol{Qq}} - \Lambda)$ by $(1-Z_+)(\Gamma'_{\boldsymbol{Qq}} - \Lambda)$ in the self-energy Σ of Eq. (11) in order to take into account the fact that the final state of the decay channel, i.e., a bare impurity in the attractive-polaron branch, exists with a probability approximately given by $(1 - Z_+)$.

The results of Γ_{PF} calculated from Eq. (16) are shown in Fig. 7. The overall behavior of Γ_{PF} as a function of δ_e is qualitatively similar for different values of $k_{\uparrow F}$. To be specific, in the regime of small negative and positive δ_e where the open-channel is detuned above the closed channel, the decay of the repulsive polaron is dominated by the closed channel. The decay rate increases as the system is tuned further towards large positive δ_e. On the other hand, in the regime of small positive and large negative δ_e where the open channel is energetically favorable, the decay rate is open-channel dominated and increases with further decrease in δ_e. The competition between the two channels thus gives rise to a nonmonotonic behavior of Γ_{PF}, which features a sharp dip when the two channels are nearly degenerate giving rise to a resonantly enhanced inter-channel scattering. On moving further towards the BCS limit of large negative δ_e, the decay rate first starts to drop due to the decreasing quasiparticle residue, Z_+, as shown in Fig. 6(c), and finally becomes undefined as the repulsive polaron branch eventually merges into the molecule-hole continuum as illustrated in Fig. 5, where the repulsive polaron is no longer a well-defined quasiparticle.

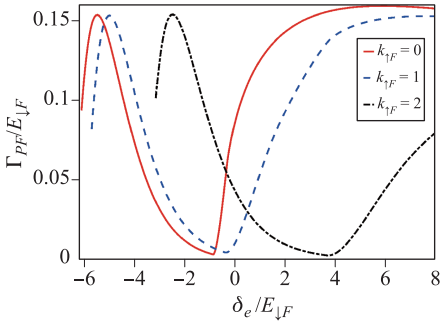

Fig. 7 The decay rate from repulsive polaron to bare fermions, showing a non-monotonic behavior with δ_e. With increasing $k_{\uparrow F}$, the minimal value of the decay rate shifts to compensate the relative offset of Fermi energy $E_{\uparrow F}$. The dip also becomes less sharp due to the fluctuation effect around the Fermi level.

5 Conclusion

We studied the impurity problem of Fermi gases near an OFR, where an atom in the $|e\uparrow\rangle$ state is immersed inside two Fermi seas filled by the two $|g\rangle$ states. By calculating the energies of the molecule and attractive polaron with zero center-of-mass momentum $\boldsymbol{Q} = 0$, we confirmed a polaron-to-molecule transition by crossing an OFR, whose exact location was shifted due to the presence of Fermi level $E_{\uparrow F}$ in the closed channel. We further studied the properties of the attractive polaron and molecule states by characterizing the wave function and the effective mass. For the repulsive polaron state, we introduced the retarded self-energy Σ to calculate the spectral function, the quasiparticle residue, the wave function distribution, the effective mass, and the decay rate. From these results, we concluded that the presence of an additional Fermi sea in the closed channel acts as its energy offset and consequently shifts the polaron-molecule transition and other key characteristics to higher values of detuning δ_e. The fluctuation around the Fermi level induced by the spin-exchange interaction also blurred the resonant-like behavior and smoothened the kink structure in various properties of the repulsive polaron. Our results can be studied experimentally using the experimental techniques in alkaline-earth(-like) atoms.

Acknowledgements This work was supported by the National Natural Science Foundation of China (Grant Nos. 11434011, 11522436, 11704408, and 11774425), and the Research Funds of Renmin University of China (Grant No. 16XNLQ03). X. Z. acknowledges support from the National Postdoctoral Program for Innovative Talents (Grant No. BX201601908) and the China Postdoctoral Science Foundation (Grant No. 2017M620991).

References

1. R. Zhang, Y. Cheng, H. Zhai, and P. Zhang, Orbital Feshbach resonance in alkali-earth atoms, *Phys. Rev. Lett.* 115(13), 135301 (2015)
2. G. Pagano, M. Mancini, G. Cappellini, L. Livi, C. Sias, J. Catani, M. Inguscio, and L. Fallani, Strongly interacting gas of two-electron fermions at an orbital Feshbach resonance, *Phys. Rev. Lett.* 115(26), 265301 (2015)
3. M. Höfer, L. Riegger, F. Scazza, C. Hofrichter, D. R. Fernandes, M. M. Parish, J. Levinsen, I. Bloch, and S.

Fölling, Observation of an orbital interaction-induced Feshbach resonance in Yb^{173}, *Phys. Rev. Lett.* 115(26), 265302 (2015)

4. Y. Cheng, R. Zhang, and P. Zhang, Orbital Feshbach resonances with a small energy gap between open and closed channels, *Phys. Rev. A* 93(4), 042708 (2016)
5. T.-S. Deng, W. Zhang, and W. Yi, Tuning Feshbach resonances in cold atomic gases with interchannel coupling, *Phys. Rev. A* 96, 050701(R) (2017)
6. M. Iskin, Two-band superfluidity and intrinsic Josephson effect in alkaline-earth-metal Fermi gases across an orbital Feshbach resonance, *Phys. Rev. A* 94, 011604(R) (2016)
7. M. Iskin, Trapped Yb^{173} Fermi gas across an orbital Feshbach resonance, *Phys. Rev. A* 95(1), 013618 (2017)
8. J. Xu, R. Zhang, Y. Cheng, P. Zhang, R. Qi, and H. Zhai, Reaching a Fermi-superfluid state near an orbital Feshbach resonance, *Phys. Rev. A* 94(3), 033609 (2016)
9. L. He, J. Wang, S. G. Peng, X. J. Liu, and H. Hu, Strongly correlated Fermi superfluid near an orbital Feshbach resonance: Stability, equation of state, and Leggett mode, *Phys. Rev. A* 94(4), 043624 (2016)
10. Y.-C. Zhang, S. Ding, and S. Zhang, Collective modes in a two-band superfluid of ultracold alkaline-earth-metal atoms close to an orbital Feshbach resonance, *Phys. Rev. A* 95, 041603(R) (2017)
11. S. Wang, J. S. Pan, X. Cui, W. Zhang, and W. Yi, Topological Fulde-Ferrell states in alkaline-earth-metal-like atoms near an orbital Feshbach resonance, *Phys. Rev. A* 95(4), 043634 (2017)
12. Y. Cheng, R. Zhang, and P. Zhang, Quantum defect theory for the orbital Feshbach resonance, *Phys. Rev. A* 95(1), 013624 (2017)
13. J. G. Chen, T. S. Deng, W. Yi, and W. Zhang, Polarons and molecules in a Fermi gas with orbital Feshbach resonance, *Phys. Rev. A* 94(5), 053627 (2016)
14. J. Xu and R. Qi, Polaronic and dressed molecular states in orbital Feshbach resonances, arXiv: 1710.00785 (2017)
15. T. S. Deng, Z. C. Lu, Y. R. Shi, J. G. Chen, W. Zhang, and W. Yi, Repulsive polarons in alkaline-earth-metal-like atoms across an orbital Feshbach resonance, *Phys. Rev. A* 97(1), 013635 (2018)
16. F. Chevy, Universal phase diagram of a strongly interacting Fermi gas with unbalanced spin populations, *Phys. Rev. A* 74(6), 063628 (2006)
17. R. Combescot, A. Recati, C. Lobo, and F. Chevy, Normal state of highly polarized Fermi gases: Simple many-body approaches, *Phys. Rev. Lett.* 98(18), 180402 (2007)
18. M. Punk, P. T. Dumitrescu, and W. Zwerger, Polaron-to-molecule transition in a strongly imbalanced Fermi gas, *Phys. Rev. A* 80(5), 053605 (2009)
19. S. Zöllner, G. M. Bruun, and C. J. Pethick, Polarons and molecules in a two-dimensional Fermi gas, *Phys. Rev. A* 83, 021603(R) (2011)
20. M. Klawunn and A. Recati, Fermi polaron in two dimensions: Importance of the two-body bound state, *Phys. Rev. A* 84(3), 033607 (2011)
21. M. M. Parish, Polaron-molecule transitions in a two-dimensional Fermi gas, *Phys. Rev. A* 83, 051603(R) (2011)
22. R. Schmidt, and T. Enss, Excitation spectra and RF response near the polaron-to-molecule transition from the functional renormalization group, *Phys. Rev. A* 83(6), 063620 (2011)
23. X. W. Guan, Polaron, molecule and pairing in one-dimensional spin-1/2 Fermi gas with an attractive delta-function interaction, *Front. Phys.* 7(1), 8 (2012)
24. C. Trefzger, and Y. Castin, Impurity in a Fermi sea on a narrow Feshbach resonance: A variational study of the polaronic and dimeronic branches, *Phys. Rev. A* 85(5), 053612 (2012)
25. M. Koschorreck, D. Pertot, E. Vogt, B. Fröhlich, M. Feld, and M. Köhl, Attractive and repulsive Fermi polarons in two dimensions, *Nature* 485(7400), 619 (2012)
26. P. Massignan, M. Zaccanti, and G. Bruun, Polarons, dressed molecules and itinerant ferromagnetism in ultracold Fermi gases, *Rep. Prog. Phys.* 77(3), 034401 (2014)
27. R. Schmidt, M. Knap, D. A. Ivanov, J. S. You, M. Cetina, and E. Demler, Universal many-body response of heavy impurities coupled to a Fermi sea: A review of recent progress, *Rep. Prog. Phys.* 81(2), 024401 (2018)
28. P. Massignan and G. M. Bruun, Repulsive polarons and itinerant ferromagnetism in strongly polarized Fermi gases, *Eur. Phys. J. D* 65(1-2), 83 (2011)
29. P. Massignan, Z. Yu, and G. M. Bruun, Itinerant ferromagnetism in a polarized two-component Fermi gas, *Phys. Rev. Lett.* 110(23), 230401 (2013)
30. C. Kohstall, M. Zaccanti, M. Jag, A. Trenkwalder, P. Massignan, G. M. Bruun, F. Schreck, and R. Grimm, Metastability and coherence of repulsive polarons in a strongly interacting Fermi mixture, *Nature* 485(7400), 615 (2012)
31. X. Cui and H. Zhai, Stability of a fully magnetized ferromagnetic state in repulsively interacting ultracold Fermi gases, *Phys. Rev. A* 81, 041602(R) (2010)
32. S. Pilati, G. Bertaina, S. Giorgini, and M. Troyer, Itinerant ferromagnetism of a repulsive atomic Fermi gas: A quantum Monte Carlo study, *Phys. Rev. Lett.* 105(3), 030405 (2010)
33. M. Cetina, M. Jag, R. S. Lous, I. Fritsche, J. T. M. Waldraven, R. Grimm, J. Levinsen, M. M. Parish, R. Schmidt, M. Knap, and E. Demler, Ultrafast many-body interferometry of impurities coupled to a Fermi sea, *Science* 354(6308), 96 (2016)
34. G. Valtolina, F. Scazza, A. Amico, A. Burchianti, A. Recati, T. Enss, M. Inguscio, M. Zaccanti, and G. Roati, Exploring the ferromagnetic behaviour of a repulsive Fermi gas through spin dynamics, *Nat. Phys.* 13(7), 704 (2017)

35. S. Mondal, D. Inotani, and Y. Ohashi, Closed-channel contribution in the BCS-BEC crossover regime of an ultracold Fermi gas with an orbital Feshbach resonance, arXiv: 1709.00154v1 (2017)

36. C. Chin, R. Grimm, P. Julienne, and E. Tiesinga, Feshbach resonances in ultracold gases, *Rev. Mod. Phys.* 82(2), 1225 (2010)

37. F. Scazza, G. Valtolina, P. Massignan, A. Recati, A. Amico, A. Burchianti, C. Fort, M. Inguscio, M. Zaccanti, and G. Roati, Repulsive Fermi polarons in a resonant mixture of ultracold Li^6 atoms, *Phys. Rev. Lett.* 118(8), 083602 (2017)